INTERNATIONAL JOURNAL FOR NUMERICAL METHODS IN ENGINEERING
Int. J. Numer. Meth. Engng. **46**, 1741–1761 (1999)

FINITE ELEMENT ANALYSIS OF BASE ISOLATED BUILDINGS SUBJECTED TO EARTHQUAKE LOADS

OMAR SALOMÓN[1], SERGIO OLLER[2] AND ALEX BARBAT[2,*]

[1] *Facultad de Ingeniería, Universidad Nacional del Nordeste, Avda. Las Heras 727, 3500 Resistencia, Chaco, Argentina*
[2] *E.T.S. Ingenieros de Caminos, Canales y Puertos, Universitat Politècnica de Catalunya, Campus Norte UPC, 08034 Barcelona, Spain*

SUMMARY

A finite element formulation modelling hyperelastic quasi-incompressible rubber-like materials (elastomers) is developed which takes into account large displacements and large elastic strains as well as inelastic effects. The capacity of laminated rubber-like materials to support high loads in compression and large displacements in shear is the principal reason for their use in devices for seismic base isolation of structures. The energy-dissipation capacity of these devices is increased by using high damping rubber, which is an elastomer incorporating carbon black particles, or having lead-plug insertion. The Ogden strain energy function has been used as a basis for the material model implemented in a total Lagrangian formulation, the strain being decomposed into its deviatory and volumetric parts and the pressure variable being condensed at element level. Mooney–Rivlin and neo-Hooke strain energy functions can also be used by simply changing the parameters of the model. The stress–strain hysteresis, which appears when these devices are subjected to dynamic or quasi-static cyclic loads, has been modelled by frequency dependent viscoelastic and plastic constitutive models. The bearings have been modelled by means of an equivalent single element capable of describing the composite behaviour of the actual isolation system. The proposed model is validated using available experimental results and it is proved to be a powerful tool in dealing with different bearings. Finally, results for a six-storey base isolated building subjected to the El Centro earthquake are given. Copyright © 1999 John Wiley & Sons, Ltd.

KEY WORDS: elastomers; rubber-like materials; seismic base isolation

1. INTRODUCTION

Base isolation systems partially uncouple a structure from seismic ground motion by means of specially designed devices inserted between the structure and its foundation. The use of base isolation devices is an advanced technique in the field of earthquake-resistant design which is being used in many countries. Among the different types of devices in existence, laminated elastomeric bearings are probably the most widely used nowadays [1–3]. They are composed of layers of rubber and steel, the rubber being vulcanized to the steel layers. The possibility of the rubber bulging is reduced by inserting the mentioned steel layers and, in this way, the vertical stiffness of

*Correspondence to: Alex Barbat, ETS Ingenieros de Caminos, Canales y Puertos, Universitat Politècnica de Catalunya, Campus Norte-Modulo c1, Gran Capitan s/n, 08034 Barcelona, Spain

Contract/grant sponsor: Universidad Nacional del Nordeste

CCC 0029-5981/99/341741–21$17.50

Received 1 September 1998
Revised 1 February 1999

the bearings is increased. The shear stiffness is not altered significantly by the presence of these layers. The most common laminated rubber bearings are: Natural Rubber Bearings (NRB), Lead Rubber Bearing (LRB) and High Damping Rubber Bearings (HRB).

The layers of rubber improve the horizontal flexibility of the system, thus increasing the fundamental period of the building, which is shifted from the predominant period of the expected earthquakes in the area, with a consequent reduction in dynamic amplifications. That results in the isolated system having a different dynamics from a conventional one.

Additionally, during a seismic event, the displacements are concentrated at the isolation devices level, the structural inter-storey drift being drastically reduced. As a consequence, the damage in structural and non-structural components is minimized. Moreover, by using high damping rubber or introducing a lead plug into the bearing, the system is provided with additional energy dissipation.

The use of laminated rubber bearings in different areas of engineering such as bridges, anti-vibration devices for machinery or base isolation system for buildings brought about extensive experimental research into them. Results have been published of tests on elastomeric bearings, on full or reduced-scale models, under low-frequency cyclic loads with amplitude up to 400 per cent shear strain of the total height of rubber and different vertical loads, and also horizontal displacements up to failure [1, 4, 5].

However, only a few analytical studies have been published [6–9], possibly owing to the difficulties of the numerical description of the real behaviour of these devices. Such a description should take into account large displacements and large non-linear elastic strains of elastomers, its incompressibility and damping characteristics, the effect of steel layers and, in certain cases, the effect of the lead plugs.

In previous studies, the analysis of base isolated buildings has generally been performed by modelling the devices as short bars with mechanical characteristics (stiffness and damping) taken from experimental tests. The superstructure has been assumed to remain within the elastic range throughout the entire numerical process. The mass has been concentrated at the floor levels with one [10, 11, 3] or three degrees of freedom per floor, that is, by using two translational and one rotational degrees of freedom [12, 13].

To the authors' knowledge, no studies have been published on the numerical analysis of buildings with elastomeric base isolation using the finite element method with constitutive models suitable for structure (reinforced concrete) and for the materials of the isolation devices (elastomers).

The only paper in which such a model has been found is Reference 7, where a finite element model is presented for the analysis of rubber systems in cable-stayed bridges. The devices were lead–rubber bearings and the behaviour of the elastomer was considered elastic, its capacity for energy dissipation not being taken into account. An 'equivalent homogeneous continuum' theory for the nonlinear behavior of elastomeric bearings was also developed [14], but again the elastomer was treated as elastic. Such an analysis is said to be far less expensive than the use of a general purpose finite element program to perform 'discrete' analysis of elastomeric bearings [15] without the corresponding convergence difficulties. However, most of the numerical examples presented in [16] consider only vertical strains due to compression and not shear strains due to horizontal cyclic loads, which are those that have utmost importance in devices for seismic base isolation.

This paper is a contribution to the numerical analysis of base isolated buildings with elastomeric base isolation systems. It develops an analytical and numerical model for the nonlinear dynamic analysis of these systems. The contribution of the proposed model is its ability to capture the highly non-linear elastic behaviour of natural and high damping rubber bearings and its energy dissipation characteristics. Non-linear behaviour is not restricted to the base isolation system because the

reinforced concrete superstructure is modelled by combining an elasto-damage constitutive model for the concrete with an elasto–plastic model for the steel bars [17, 18].

The next section presents the proposed approach to model the elastomeric part of the bearing, which is a generalized hyperelastic model for the analysis of multi-phase elastomeric materials. Mixing theory is used to insert the basic constitutive expressions for each substance on the multi-phase composite solid: viscoelasticity for rubber (Ogden elasticity in the case of static loads) and elastoplasticity for carbon black particles. The model is formulated in large strains in terms of principal stretches. Section 3 gives the finite element implementation of the proposed constitutive model, taking into account the quasi-incompressible behavior of rubber-like materials. In Section 4, the performance of the proposed formulation and its numerical implementation is illustrated by means of simple numerical simulations which are compared with experimental results. As an example of application to a base isolated structure, a six-storey reinforced concrete frame with high damping rubber bearings is analysed in Section 5. Maximum inter-storey displacements, absolute floor accelerations and overall damage indices are shown for this base isolated structure and compared with a similar fixed-base structure, both having been subjected to the N–S component of the El Centro earthquake.

2. DESCRIPTION OF THE HYPERELASTIC CONSTITUTIVE MODEL

Rubber-like materials behave as hyperelastic, incompressible and, from a macroscopic point of view, homogeneous and isotropic solids. Laboratory tests on elastomeric pads under cyclic loads show hysteretic damping in their response [4], the amplitude of which is far greater in the case of high damping rubber bearings [1]. In these devices an important proportion of carbon black particles are added to the rubber component.

These characteristics allow a phenomenologically motivated model in which no micro-mechanical considerations are taken into account. Firstly, owing to the quasi-incompressibility of rubber, the approach presented herein to model elastomeric devices assumes that the volumetric and isochoric parts of the deformation behave differently. Secondly, as hysteretic damping depends on the components of rubber, different models are considered for each substance. Next, mixing theory is used to insert the basic constitutive expressions for each component on a multi-phase composite solid [17]. The overall physical behaviour is influenced by the mechanical characteristics of each simple component according to its volume proportion. Kinematic compatibility at all time instants is accepted as a closing equation. Finally, as temperature is not a variable included in the strain energy functions, the current development is limited to stable thermal conditions.

As we are dealing with a hyperelastic-based model, stresses and tangent moduli are derivable from strain energy functions W

$$\mathbf{S} = \frac{\partial W}{\partial \mathbf{E}}, \quad \mathbb{C} = \frac{\partial^2 W}{\partial \mathbf{E} \otimes \partial \mathbf{E}} \tag{1}$$

where $\mathbf{S}$ is the second Piola–Kirchhoff stress tensor, $\mathbb{C}$ is the tangent moduli tensor at reference configuration and $\mathbf{E}$ is the Green strain tensor

$$\mathbf{E} = \tfrac{1}{2}(\mathbf{C} - \mathbf{I}), \quad \mathbf{C} = \mathbf{F}^{\mathrm{T}}\mathbf{F} \tag{2}$$

$\mathbf{C}$ is the right Cauchy–Green tensor, $\mathbf{F}$ the deformation gradient and $\mathbf{I}$ the identity second order tensor.

To decouple isochoric and dilational response, $\mathbf{F}$ is split multiplicatively as follows:

$$\mathbf{F} = \mathbf{F}_{\text{vol}}\,\bar{\mathbf{F}}, \quad \mathbf{F}_{\text{vol}} = J^{1/3}\mathbf{1}, \quad \bar{\mathbf{F}} = J^{-1/3}\mathbf{F} \tag{3}$$

where $J = \det[\mathbf{F}] = \det[\mathbf{F}_{\text{vol}}]$, $\det[\bar{\mathbf{F}}] = 1$.

Using (3), the stored energy function can be expressed as an additive split of the deviatoric and volumetric parts

$$W = W(J) + \bar{W}(\bar{\mathbf{F}}) \tag{4}$$

The uncoupled stored energy function produces uncoupled stress–strain relations. Associated with the volumetric strain, there is the hydrostatic pressure p

$$p = \partial_J W(J) = W'(J) \rightarrow \boldsymbol{\sigma}_{\text{v}} = W'(J)\mathbf{1} \tag{5}$$

or, in terms of the second Piola–Kirchhoff stress tensor, $\mathbf{S}_{\text{v}} = J\mathbf{F}^{-1}\boldsymbol{\sigma}_{\text{v}}\mathbf{F}^{-\text{T}}$, and considering that the Cauchy stress tensor, $\boldsymbol{\sigma}_{\text{v}}$, has non-zero elements only in its diagonal, $\mathbf{S}_{\text{v}}$ can be expressed as $\mathbf{S}_{\text{v}} = J\mathbf{F}^{-1}\mathbf{F}^{-\text{T}}\boldsymbol{\sigma}_{\text{v}} = J\mathbf{C}^{-1}\boldsymbol{\sigma}_{\text{v}}$, that is

$$\mathbf{S}_{\text{v}} = JW'(J)\mathbf{C}^{-1} \tag{6}$$

For the volumetric part of the stored energy function the following expression is used:

$$W(J) = 1/2\kappa(J-1)^2 \quad \text{with } J = I_3^{1/2} \quad \text{and} \quad I_3 = \det(\mathbf{C}) \tag{7}$$

κ being the material bulk modulus at the reference configuration. In this way

$$W'(J) = p = \kappa(J-1) \quad \text{and} \quad W''(J) = \kappa \tag{8}$$

and $\mathbb{C}_{\text{vol}}$, the volumetric part of the constitutive tensor at reference configuration, is

$$\mathbb{C}_{\text{vol}} = [JW'(J)]'J\mathbf{C}^{-1} \otimes \mathbf{C}^{-1} - JW'(J)\mathbb{I}_{C^{-1}} \tag{9}$$

Equations (5)–(9) are suitable for dealing with the volumetric part of the formulation. With regard to its isochoric part, considering (3) and (4) and the closing equation (that is, kinematics compatibility at all times) we can write

$$\bar{\mathbf{F}}_{\text{rubber}} \equiv \bar{\mathbf{F}}_{\text{particles}} \equiv \bar{\mathbf{F}} \tag{10}$$

It must now be considered that the behaviour of rubber particles is not the same. Rubber is assumed to respond to a viscoelastic basic constitutive model, with $\bar{W}(\bar{\mathbf{F}})$ valid for infinitely slow strain histories $\bar{W}^{\infty}(\bar{\mathbf{F}})$. For time-dependent strains, the energy function W includes certain internal variables which take into account the viscoelastic effects

$$\bar{W}_{\text{rubber}} = \bar{W}_{\text{ve}}(\bar{\mathbf{F}}, \alpha) \tag{11}$$

Carbon black particles are assumed to be elastoplastic, and $\bar{\mathbf{F}}$ is therefore split multiplicatively

$$\bar{\mathbf{F}} = \bar{\mathbf{F}}^{\text{e}}\,\bar{\mathbf{F}}^{\text{p}} \rightarrow \bar{\mathbf{b}}^{\text{e}} = \bar{\mathbf{F}}^{\text{e}}\,\bar{\mathbf{F}}^{\text{e T}}$$

$\bar{\mathbf{b}}^{\text{e}}$ being the elastic part of the left Cauchy–Green tensor, which is used to write an energy function for the particles component

$$\bar{W}_{\text{particles}} = \bar{W}_{\text{ep}}(\bar{\mathbf{b}}^{\text{e}}, \boldsymbol{\xi}) \tag{12}$$

Using mixing theory, the overall physical behaviour in (1) is given by an additive form

$$W = W(J) + kr[\bar{W}_{\text{ve}}(\bar{\mathbf{F}}, \alpha)] + kp[\bar{W}_{\text{ep}}(\bar{\mathbf{b}}^{\text{e}}, \xi)] \tag{13}$$

where kr and kp are the volume proportion of rubber and carbon black particles. If we now consider this additive expression of the strain energy function, the stress tensor in (1) becomes

$$\mathbf{S} = \mathbf{S}_{\text{vol}} + kr\,\bar{\mathbf{S}}_{\text{ve}} + kp\,\bar{\mathbf{S}}_{\text{ep}} \tag{14}$$

2.1. Strain energy functions for rubber-like materials

Strain energy functions W for rubber-like materials are frequently based on principle invariants of $\mathbf{C}$. The most widely used are Mooney–Rivlin models, which in their generalized form are expressed as

$$W = \sum_{r=0}^{\infty}\sum_{s=0}^{\infty}\sum_{t=0}^{\infty} C_{rs}(I_1 - 3)^r(I_2 - 3)^s(I_3 - 1)^t \tag{15}$$

where I_{i} are the invariants and C_{rs} are material constants. Since these invariants can be expressed as

$$\begin{aligned} I_1 &= \text{tr}(\mathbf{C}) = \lambda_1^2 + \lambda_2^2 + \lambda_3^2 \\ I_2 &= 1/2(I_1^2 - \text{tr}(\mathbf{C}^2)) \\ &= \lambda_2^2 \cdot \lambda_3^2 + \lambda_3^2 \cdot \lambda_1^2 + \lambda_1^2 \cdot \lambda_2^2 \\ I_3 &= \det(\mathbf{C}) = \lambda_1^2 \cdot \lambda_2^2 \cdot \lambda_3^2 \end{aligned} \tag{16}$$

where λ_i are principal values of the right stretch tensor $\mathbf{U}(\mathbf{U} = \mathbf{C}^{1/2})$, the strain energy function can take the form [19]

$$W(\lambda_1, \lambda_2, \lambda_3) = \sum_{p=1}^{N} \frac{\mu_p}{\alpha_p}(\lambda_1^{\alpha_p} + \lambda_2^{\alpha_p} + \lambda_3^{\alpha_p} - 3) \tag{17}$$

where μ_p and α_p are material parameters. Strain energy function (17), which is used in this study, includes Mooney–Rivlin models as a particular case.

Another way of representing the same strain energy function uses the principal values (L_i) of $\mathbf{C}$, that is

$$W(L_1, L_2, L_3) = \sum_{p=1}^{N} \frac{\mu_p}{\alpha_p}(L_1^{\alpha_p/2} + L_2^{\alpha_p/2} + L_3^{\alpha_p/2} - 3) \tag{18}$$

From (1) and using the chain rule

$$\mathbf{S} = 2\frac{\partial \bar{W}(C)}{\partial \mathbf{C}} = \sum_{A=1}^{3} \frac{1}{\lambda_A}\frac{\partial W(\lambda_i)}{\partial \lambda_A}\frac{\partial(\lambda_A^2)}{\partial \mathbf{C}} \tag{19}$$

For totally incompressible materials $I_3 = \lambda_1^2\lambda_2^2\lambda_3^2 = 1$; $L_1L_2L_3 = 1$.

Since $\bar{\mathbf{F}}$ in (3) has the same characteristic subspaces as $\mathbf{F}$, its spectral decomposition can be performed as

$$\bar{\mathbf{F}} = \sum_{A=1}^{3} \bar{\lambda}_A \mathbf{n}_A \otimes \mathbf{N}_A, \quad \bar{\lambda}_A = J^{-1/3}\lambda_A, \quad \bar{\lambda}_1\bar{\lambda}_2\bar{\lambda}_3 = 1 \tag{20}$$

Using equation (20), the spectral decompositions of $\bar{\mathbf{C}} = \bar{\mathbf{F}}^{\mathrm{T}}\bar{\mathbf{F}}$ and $\bar{\mathbf{b}} = \bar{\mathbf{F}}\bar{\mathbf{F}}^{\mathrm{T}}$ can be expressed as

$$\bar{\mathbf{C}} = \sum_{A=1}^{3} \bar{\lambda}_A^2 \mathbf{N}_A \otimes \mathbf{N}_A, \qquad \bar{\mathbf{b}} = \sum_{A=1}^{3} \bar{\lambda}_A^2 \mathbf{n}_A \otimes \mathbf{n}_A, \quad \|\mathbf{N}_A\| = \|\mathbf{n}_A\| = 1 \tag{21}$$

which depend on the principal directions $\mathbf{N}_A$ and $\mathbf{n}_A$. The principal directions $\mathbf{N}_A$ are also useful to calculate $\partial_{\mathbf{C}}(\lambda_A^2)$ in equation (19)

$$\frac{\partial(\lambda_A^2)}{\partial \mathbf{C}} = \mathbf{N}_A \otimes \mathbf{N}_A \tag{22}$$

and allow the deviatoric elastic part of the second Piola–Kirchhoff $\bar{\mathbf{S}}$ and Cauchy $\bar{\boldsymbol{\sigma}}$ stresses to be expressed as

$$\begin{aligned} \bar{\mathbf{S}} &= \sum_{A=1}^{3} \beta_A \mathbf{M}_A, \quad \mathbf{M}_A = \bar{\lambda}_A^{-2} \mathbf{N}_A \otimes \mathbf{N}_A \\ \bar{\boldsymbol{\sigma}} &= \frac{1}{J} \sum_{A=1}^{3} \beta_A \mathbf{m}_A, \quad \mathbf{m}_A = \mathbf{n}_A \otimes \mathbf{n}_A = \mathbf{F}\mathbf{M}_A\mathbf{F}^{\mathrm{T}} \end{aligned} \tag{23}$$

where

$$\beta_A = \lambda_A \partial W / \partial \lambda_A \tag{24}$$

and $\mathbf{N}_A \otimes \mathbf{N}_A$ and $\mathbf{n}_A \otimes \mathbf{n}_A$ can be expressed from the tensors $\mathbf{C}$ and $\mathbf{b}$ [20, 21]

$$\begin{aligned} \mathbf{N}_A \otimes \mathbf{N}_A &= \lambda_A^2 \frac{\mathbf{C} - (I_1 - \lambda_A^2)\mathbf{1} + I_3 \lambda_A^{-2} \mathbf{C}^{-1}}{D_A} \\ \mathbf{n}_A \otimes \mathbf{n}_A &= \frac{\mathbf{b}^2 - (I_1 - \lambda_A^2)\mathbf{b} + I_3 \lambda_A^{-2} \mathbf{1}}{D_A} \\ D_A &= 2\lambda_A^4 - I_1 \lambda_A^2 + I_3 \lambda_A^{-2} \end{aligned} \tag{25}$$

With the derivatives of equation (19), by applying the chain rule and equation (22), we get from equation (23) the deviatoric elastic part of the constitutive tensor in terms of the principal stretches at the reference configuration

$$\bar{\mathbb{C}} = \sum_{A=1}^{3} \left[\sum_{B=1}^{3} \gamma_{AB} \mathbf{M}_A \otimes \mathbf{M}_B \right] + \sum_{A=1}^{3} 2\beta_A \frac{\partial \mathbf{M}_A}{\partial \mathbf{C}} \tag{26}$$

where β_A was given in equation (24)

$$\gamma_{AB} = \gamma_{BA} = \lambda_B \frac{\partial}{\partial \lambda_B} \left(\lambda_A \frac{\partial w}{\partial \lambda_B} \right) \tag{27}$$

and $\partial_{\mathbf{C}} \mathbf{M}_{\mathbf{A}}$ is obtained from equation (25a), using equation (22) and the following relations:

$$\frac{\partial \lambda_A}{\partial I_1} = \frac{1}{2} \frac{\partial \lambda_A^3}{D_A}, \quad \frac{\partial \lambda_A}{\partial I_2} = -\frac{1}{2} \frac{\partial \lambda_A}{D_A}, \quad \frac{\partial \lambda_A}{\partial I_3} = \frac{1}{2} \frac{\partial \lambda_A^{-1}}{D_A} \tag{28}$$

where D_A is given by equation (25c). In this way, we arrive at

$$\begin{aligned}\frac{\partial \mathbf{M_A}}{\partial \mathbf{C}} &= \frac{1}{D_A}[\mathbb{I} - \mathbf{1}\otimes\mathbf{1} + I_3\lambda_A^{-2}(\mathbf{C}^{-1}\otimes\mathbf{C}^{-1} - \mathbb{I}_{C^{-1}})] \\ &+ \frac{1}{D_A}[\lambda_A^2(\mathbf{1}\otimes\mathbf{M}_A + \mathbf{M}_A\otimes\mathbf{1}) - 1/2D'_A\lambda_A\mathbf{M}_A\otimes\mathbf{M}_A] \\ &- \frac{1}{D_A}[I_3\lambda_A^{-2}(\mathbf{C}^{-1}\otimes\mathbf{M}_A + \mathbf{M}_A\otimes\mathbf{C}^{-1})] \end{aligned} \tag{29}$$

where $\mathbb{I}$ is the fourth-order identity tensor and

$$\begin{aligned} D'_A &= 8\lambda_A^3 - 2I_1\lambda_A - 2I_3\lambda_A^{-3} \\ (I_{C^{-1}})_{ABCD} &= \tfrac{1}{2}(C_{AC}^{-1}C_{BD}^{-1} + C_{AD}^{-1}C_{BC}^{-1}) \end{aligned} \tag{30}$$

The deviatoric elastic part of the constitutive tensor at the spatial configuration $\bar{\mathbb{c}}$ is obtained by a push-forward of its material form $\bar{\mathbb{C}}$, expressed in equation (26)

$$\bar{\mathbb{c}} = \frac{1}{J}\sum_{A=1}^{3}\left[\sum_{B=1}^{3}\gamma_{AB}\mathbf{m}_A\otimes\mathbf{m}_B\right] + \frac{2}{J}\sum_{A=1}^{3}2\beta_A\frac{\partial\mathbf{m}_A}{\partial\mathbf{g}} \tag{31}$$

where, as in equation (26), β_A is given by equation (24) and γ_{AB} by equation (27). The expression $\partial_g\mathbf{m}_A = \mathbf{F}\partial_C\mathbf{M}_A\mathbf{F}^{\mathrm{T}}$ has the form

$$\begin{aligned}\frac{\partial\mathbf{m}_A}{\partial\mathbf{g}} &= \frac{1}{D_A}[\mathbb{I}_b - \mathbf{b}\otimes\mathbf{b} + I_3\lambda_A^{-2}(\mathbf{1}\otimes\mathbf{1} - \mathbb{I})] \\ &+ \frac{1}{D_A}\left[\lambda_A^2(\mathbf{b}\otimes\mathbf{m}_A + \mathbf{m}_A\otimes\mathbf{b}) - \frac{1}{2}D'_A\lambda_A\mathbf{m}_A\otimes\mathbf{m}_A\right] \\ &- \frac{1}{D_A}[I_3\lambda_A^{-2}(\mathbf{1}\otimes\mathbf{m}_A + \mathbf{m}_A\otimes\mathbf{1})] \end{aligned} \tag{32}$$

with

$$(I_b)_{abcd} = \tfrac{1}{2}(b_{ac}b_{bd} + b_{ad}b_{bc}) \tag{33}$$

Note that equations (19)–(33) are valid for any stored energy function and therefore they represent a general formulation of isotropic large strain elasticity in terms of the principal stretches. The explicit forms of β_A and γ_{AB} for the Ogden strain energy function are

$$\begin{aligned} \beta_A &= \sum_{i=1}^{N}\frac{\mu_i}{\alpha_i}\left[\lambda_A^{\alpha_i} - \frac{1}{3}\sum_{B=1}^{3}\lambda_B^{\alpha_i}\right] \\ \text{If } A = B \rightarrow \gamma_{AB} &= \sum_{i=1}^{N}\mu_i\left[\frac{1}{3}\lambda_A^{\alpha_i} + \frac{1}{9}\sum_{C=1}^{3}\lambda_C^{\alpha_i}\right] \\ \text{If } A \neq B \rightarrow \gamma_{AB} &= \sum_{i=1}^{N}\mu_i\left[-\frac{1}{3}\lambda_A^{\alpha_i} - \frac{1}{3}\lambda_B^{\alpha_i} + \frac{1}{9}\sum_{C=1}^{3}\lambda_C^{\alpha_i}\right] \end{aligned} \tag{34}$$

2.2. *Viscoelasticity*

To take into account the viscous effects of polymer chain relaxation, finite strain viscoelasticity is considered [22–24]. For infinitely slow deformation histories the response of the material is

elastic, according to equation (23). For arbitrary deformation histories the material exhibits fading memory described by the hereditary integral

$$\bar{\mathbf{S}} = \int_0^t g(t-s)\frac{\mathrm{d}}{\mathrm{d}s}\bar{\mathbf{S}}\,\mathrm{d}s \tag{35}$$

where $g(t) = 1 + \sum_{k=1}^{N} \gamma_k \exp(-t/\tau_k)$ is the relaxation function. γ_k is the stiffness of the k Maxwell element included in the model and τ_k its relaxation time. The response of the Maxwell elements can be expressed as

$$\mathbf{H}_k^{n+1} = \int_0^{t_n+1} \exp\left(-\frac{t_{n+1}-s}{\tau_k}\right)\frac{\mathrm{d}\bar{\mathbf{S}}(s)}{\mathrm{d}s}\,\mathrm{d}s \tag{36}$$

The exponential convolution integral can be estimated using the midpoint rule to give

$$\mathbf{H}_k^{n+1} = \exp\left(\frac{-\Delta t}{\tau_k}\right)\mathbf{H}_k^n + \frac{1-\exp(-\Delta t/\tau_k)}{\Delta t/\tau_k}[\,\bar{\mathbf{S}}^{n+1} - \bar{\mathbf{S}}^n] \tag{37}$$

The stress response $\bar{\mathbf{S}}_{\mathrm{ve}}$ in (14) is defined as a superposition of the equilibrium, $\bar{\mathbf{S}}$, given by (23) and the non-equilibrium stress contributions, $\mathbf{H}$

$$\bar{\mathbf{S}}_{\mathrm{ve}} = \bar{\mathbf{S}} + \sum_{k=1}^{N} \mathbf{H}_k \tag{38}$$

2.3. Elastoplasticity

In order to take into account the behaviour of carbon black particles in rubber-like materials, finite strains plasticity is now considered [23, 24]. The formulation is based on multiplicative decomposition of the deformation gradient $\mathbf{F} = (J^{1/3}\mathbf{I})\bar{\mathbf{F}}^{\mathrm{e}}\bar{\mathbf{F}}^{\mathrm{p}}$, maintains the structure of the classical infinitesimal plasticity models [25] and preserves exactly the plastic volume changes for pressure insensitive yield criteria.

A trial elastic state for the prescribed strain increments is computed first

$$\bar{\mathbf{b}}^{\mathrm{e\,tr}} = \bar{\mathbf{F}}^{\mathrm{e}}\bar{\mathbf{F}}^{\mathrm{e\,T}} = \bar{\mathbf{F}}\bar{\mathbf{C}}^{\mathrm{p}-1}\bar{\mathbf{F}}^{\mathrm{T}} \tag{39}$$

where $\bar{\mathbf{C}}^{\mathrm{p}} = \bar{\mathbf{F}}^{\mathrm{p\,T}}\bar{\mathbf{F}}^{\mathrm{p}}$ is a plastic strain tensor. After the spectral decomposition of $\bar{\mathbf{b}}^{\mathrm{e\,tr}}$ as expressed in (21), the principal elastic logarithmic stretches are defined by

$$\bar{\varepsilon}_A^{\mathrm{e\,tr}} = \log[\bar{\lambda}_A^{\mathrm{e\,tr}}], \quad A = 1,2,3 \tag{40}$$

Choosing for $\bar{W}_{\mathrm{ep}}$ in (12) the uncoupled form, which is quadratic in principal elastic logarithmic stretches

$$\bar{W}_{\mathrm{ep}}(\bar{\varepsilon}_A^{\mathrm{e}}, \xi) = \mu[\bar{\boldsymbol{\varepsilon}}^{\mathrm{e}} \cdot \bar{\boldsymbol{\varepsilon}}^{\mathrm{e}}] + K(\xi) \tag{41}$$

the principal isochoric stress $\boldsymbol{\beta} = \partial_{\varepsilon}\bar{W}_{\mathrm{ep}}(\bar{\varepsilon}_A^{\mathrm{e}}, \xi)$ is

$$\boldsymbol{\beta}^{\mathrm{tr}} = 2\mu\bar{\boldsymbol{\varepsilon}}^{\mathrm{e\,tr}} \tag{42}$$

Consequently, the trial state $\boldsymbol{\beta}^{\mathrm{tr}}$ is projected onto the elastic domain, defining the actual stress $\boldsymbol{\beta}$ at each Gauss point of the finite element. The von Mises yield criterion used to define the elastic domain is written in the classical form

$$\phi(\boldsymbol{\tau}, \xi) = \|\mathrm{dev}[\boldsymbol{\tau}]\| - \sqrt{\tfrac{2}{3}}[\sigma_Y + K'(\xi)] \leqslant 0 \tag{43}$$

where σ_Y is the flow stress, ξ is the equivalent plastic strain, $\|\mathrm{dev}[\boldsymbol{\tau}]\|$ is the square root of the J_2 invariant of the Kirchhoff stress $\boldsymbol{\tau}$, and $K(\xi)$ an internal variable characterizing the isotropic hardening response of the material. Therefore

$$\boldsymbol{\beta} = \boldsymbol{\beta}^{\mathrm{tr}} - 2\mu\Delta\gamma\mathbf{v} \tag{44}$$

where $\mathbf{v}$ is the unit outward normal to the von Mises cylinder in principal stress space

$$\mathbf{v} = \boldsymbol{\beta}/\|\boldsymbol{\beta}\|, \quad \|\mathrm{dev}[\boldsymbol{\tau}]\| = \|\boldsymbol{\beta}\|$$

and

$$\xi = \xi + \sqrt{\tfrac{2}{3}}\Delta\gamma, \quad \Delta\gamma \geqslant 0 \tag{45}$$

The consistency condition $\phi_{n+1} = 0$ provides the scalar equation for $\Delta\gamma \geqslant 0$ during plastic loading

$$\phi_{n+1} = \phi^{\mathrm{tr}}_{n+1} - 2\mu\Delta\gamma - \sqrt{\tfrac{2}{3}}[K'(\xi_n + \sqrt{\tfrac{2}{3}}\Delta\gamma) - K'(\xi_n)] = 0 \tag{46}$$

Kinematic hardening can be incorporated considering a von Mises yield criterion in the form

$$\phi(\boldsymbol{\beta} - \boldsymbol{\xi}, \xi) = \|\boldsymbol{\beta} - \boldsymbol{\xi}\| - \sqrt{\tfrac{2}{3}}[\sigma_Y + K'(\xi)] \leqslant 0 \tag{47}$$

where $\boldsymbol{\xi}$ represents the vector of the principal values of the back-stress tensor

$$\boldsymbol{\xi}_{n+1} = \boldsymbol{\xi}_n + \tfrac{2}{3}\Delta\gamma H\mathbf{v}_{n+1} \tag{48}$$

H being the kinematic hardening modulus. The normal to the von Mises cylinder, $\mathbf{v}$, is now

$$\mathbf{v}_{n+1} = \partial_\beta\phi_{n+1} = \frac{\boldsymbol{\zeta}_{n+1}}{\|\boldsymbol{\zeta}_{n+1}\|}, \quad \boldsymbol{\zeta} = \boldsymbol{\beta} - \boldsymbol{\xi} \tag{49}$$

Equation (46) is now expressed as

$$\phi^{\mathrm{tr}}_{n+1} - 2\mu\Delta\gamma\left[1 + \frac{H}{3\mu}\right] - \sqrt{\frac{2}{3}}\left[K'\left(\xi_n + \sqrt{\frac{2}{3}}\Delta\gamma\right) - K'(\xi_n)\right] = 0 \tag{50}$$

The elastoplastic constitutive tensor $\mathbb{C}_{\mathrm{ep}}$ associated with the return mapping takes the form [25]

$$\begin{aligned} \bar{\mathbb{C}}_{\mathrm{ep}} &= 2\mu[s_{n+1}(\mathbf{I}_3 - \tfrac{1}{3}\mathbf{1}\otimes\mathbf{1}) - \delta_{n+1}(\mathbf{v}_{n+1}\otimes\mathbf{v}_{n+1})] \\ s_{n+1} &= 1 - \frac{2\mu\Delta\gamma}{\|\boldsymbol{\zeta}^{\mathrm{tr}}_{n+1}\|}, \quad \delta_{n+1} = \frac{1}{1 + (K'' + H)/3\mu} - \frac{2\mu\Delta\gamma}{\|\boldsymbol{\zeta}^{\mathrm{tr}}_{n+1}\|} \end{aligned} \tag{51}$$

By solving equation (44) and using (42), the logarithmic elastic state of deformation is known. The final elastic tensor $\bar{\mathbf{b}}^{\mathrm{e}}$, which will be used for the plastic strain tensor $\bar{\mathbf{C}}^{\mathrm{p}}$ in (39), is obtained by an exponential algorithm

$$\bar{\mathbf{b}}^{\mathrm{e}} = \sum_{A=1}^{3} \bar{\lambda}_A^{\mathrm{e}\,2} \mathbf{n}_A \otimes \mathbf{n}_A, \quad \bar{\lambda}_A^{\mathrm{e}} = \exp(\bar{\lambda}_A), \quad \bar{\mathbf{C}}^{\mathrm{p}\,-1} = \bar{\mathbf{F}}^{-1}\, \bar{\mathbf{b}}^{\mathrm{e}} \bar{\mathbf{F}}^{-\mathrm{T}} \tag{52}$$

$\bar{\mathbf{S}}_{\mathrm{ep}}$ in (14) is given by a pull-back of $\boldsymbol{\beta}$ in (44)

$$\bar{\mathbf{S}}_{\mathrm{ep}} = J \bar{\mathbf{F}}^{-1} \boldsymbol{\beta} \bar{\mathbf{F}}^{-\mathrm{T}} \tag{53}$$

and the constitutive tensor at reference configuration $\bar{\mathbb{C}}_{\mathrm{ep}}$ is given by a pull-back of $\bar{\mathbb{c}}_{\mathrm{ep}}$ in (51).

3. FINITE ELEMENT IMPLEMENTATION

It is well known that a displacement-based finite element method presents difficulties (locking, ill-conditioning of the stiffness matrix, etc.) in the analysis of quasi-incompressible materials [21, 26–29]. To overcome these difficulties several formulations have been proposed [21, 27, 29]. All of them are based on the split of the deformation gradient tensor in its isochoric and dilational parts and can be grouped into the *multifield* or *mixed principles* and *reduced selective integration penalty approach* methods.

In this work a two field formulation (displacement and pressure) is used. Rubber material is represented by a particular formulation of displacement–pressure finite elements in a total Lagrangian formulation [26, 28]. The equations of motion for a finite element are

$$\begin{bmatrix} \mathbf{K}_{uu} & \mathbf{K}_{up} \\ \mathbf{K}_{pu} & \mathbf{K}_{pp} \end{bmatrix} \begin{bmatrix} \mathbf{u} \\ \mathbf{p} \end{bmatrix} = \begin{bmatrix} \mathbf{R} \\ \mathbf{0} \end{bmatrix} - \begin{bmatrix} \mathbf{F}_u \\ \mathbf{F}_p \end{bmatrix} \tag{54}$$

$$\begin{aligned} \mathbf{K}_{uu} &= \int_V \mathbf{B}_{\mathrm{L}}^{\mathrm{T}} \mathbf{C}_{uu} \mathbf{B}_{\mathrm{L}}\, \mathrm{d}V + \int_V \mathbf{B}_{\mathrm{NL}}^{\mathrm{T}} \mathbf{S} \mathbf{B}_{\mathrm{NL}}\, \mathrm{d}V \\ \mathbf{K}_{up} &= \int_V \mathbf{B}_{\mathrm{L}}^{\mathrm{T}} \mathbf{C}_{up}\, \mathrm{d}V = \mathbf{K}_{pu}^{\mathrm{T}}, \quad \mathbf{K}_{pp} = \int_V C_{pp}\, \mathrm{d}V \\ \mathbf{F}_u &= \int_V \mathbf{B}_{\mathrm{L}}^{\mathrm{T}} \mathbf{S}\, \mathrm{d}V, \quad \mathbf{F}_p = \int_V -C_{pp}(\bar{p} - \tilde{p}) \frac{\partial \tilde{p}}{\partial \tilde{p}}\, \mathrm{d}V = \mathbf{0} \end{aligned} \tag{55}$$

where $\mathbf{R}$ are nodal external forces, $\mathbf{B}_{\mathrm{L}}$ and $\mathbf{B}_{\mathrm{NL}}$ are the linear and nonlinear strain–displacement transformation matrices [28] and $\mathbf{S}$ the second Piola–Kirchhoff tensor

$$\mathbf{S} = \bar{\mathbf{S}} + C_{pp}(\bar{p} - \tilde{p}) \frac{\partial \bar{p}}{\partial E_{kl}} \tag{56}$$

$$\begin{aligned} C_{pp} &= -\frac{1}{\kappa}, \quad \mathbf{C}_{up} = -C_{pp} \frac{\partial \bar{p}}{\partial E_{kl}} \\ \mathbf{C}_{uu} &= \bar{\mathbb{C}} + C_{pp} \frac{\partial \bar{p}}{\partial E_{kl}} \frac{\partial \bar{p}}{\partial E_{rs}} + C_{pp}(\bar{p} - \tilde{p}) \frac{\partial \bar{p}}{\partial E_{kl} \partial E_{rs}} \end{aligned} \tag{57}$$

In these equations $\bar{\mathbf{S}}$ and $\bar{\mathbb{C}}$ are the isochoric part of the second Piola–Kirchhoff tensor and the tangent modulus at reference configuration in terms of principal stretches, respectively. The bulk

modulus κ is treated as a penalty parameter and, with the aim of forcing a quasi-constant volume deformation, it must have a sufficiently large value. $\mathbf{E}$ is the right Green–Lagrange tensor.

Choosing $W(J)=\frac{1}{2}\kappa(J_3-1)^2$ for (7), the pressure $\bar{p}$ obtained from the displacement field is $\bar{p}=\kappa(J_3-1)$ and its derivatives are

$$\frac{\partial \bar{p}}{\partial E_{kl}} = -\kappa J_3 \mathbf{C}^{-1} \quad \text{and} \quad \frac{\partial \bar{p}}{\partial E_{kl}\partial E_{rs}} = \kappa J_3 \mathbf{C}^{-1}\otimes\mathbf{C}^{-1} - \kappa J_3^{-1} 2\mathbf{Q} \tag{58}$$

where $J_3=I_3^{1/2}$, $\mathbf{C}$ is the right Cauchy–Green tensor and $\mathbf{Q}$ is

$$[Q]=\begin{bmatrix} 0 & C_{33} & C_{22} & 0 & -C_{23} & 0 \\ & 0 & C_{11} & 0 & 0 & -C_{13} \\ & & 0 & -C_{12} & 0 & 0 \\ & & & -0{\cdot}5C_{33} & 0{\cdot}5C_{31} & 0{\cdot}5C_{23} \\ & \text{sym.} & & & -0{\cdot}5C_{11} & 0{\cdot}5C_{12} \\ & & & & & -0{\cdot}5C_{22} \end{bmatrix} \tag{59}$$

Starting from $\bar{p}$ at each Gauss point, an average pressure $\tilde{p}$ at element level is obtained. A single pressure point is considered for each element, with the pressure assumed constant over the element. Static condensation is used to eliminate the pressure degree of freedom at element level. From the second equation (54) we obtain $\mathbf{p}=\mathbf{K}_{pp}^{-1}(-\mathbf{F}_p-\mathbf{K}_{up}^{\mathrm{T}}\mathbf{u})$ and replacing this in first equation (54)

$$\begin{aligned} \mathbf{K}\mathbf{u} &= \mathbf{R}-\mathbf{F} \\ \mathbf{K} &= \mathbf{K}_{uu}-\mathbf{K}_{up}\mathbf{K}_{pp}^{-1}\mathbf{K}_{up}^{\mathrm{T}} \\ \mathbf{F} &= \mathbf{F}_u-\mathbf{K}_{up}\mathbf{K}_{pp}^{-1}\mathbf{F}_p^{\mathrm{T}} \end{aligned} \tag{60}$$

4. MODEL VALIDATION

In order to test the proposed model, a single element has been analysed under plain strain homogeneous simple shear deformation. The values of the elastic material constants employed in (18) were chosen as shown in Table I.

Horizontal displacement was applied up to 550 per cent of shear strain. A plot of shear stress versus the amount of shear strain is shown in Figure 1. It should be compared with the experimental results [1] for natural and high damping rubber bearings shown in Figure 2.

Two other cases are analysed with cyclic load having frequencies of 0·01 Hz and amplitudes from ± 25 per cent to ± 400 per cent of the shear strain. For the first one, the material is considered to be natural rubber and modelled as viscoelastic with $v=0{\cdot}5$, while for the second the material is considered to be rubber with high damping modelled as visco-elasto–plastic, with $v=0{\cdot}9$ and

Table I. Material parameters for elastomer

G (kg/cm^2)	μ_1	μ_2	μ_3	α_1	α_2	α_3
4·5	1·03	0·002	−0·02	1·9	5·9	−1·6

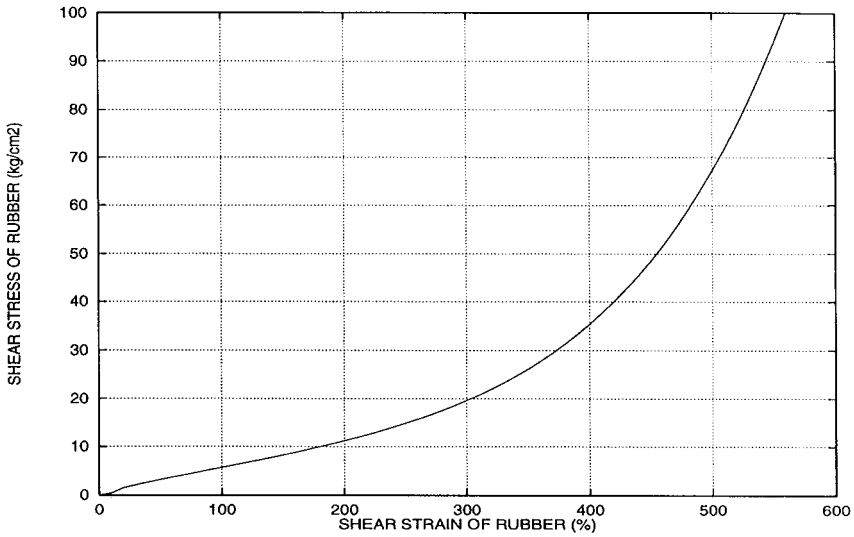

Figure 1. Relationship between shear stress and shear strain. Numerical model

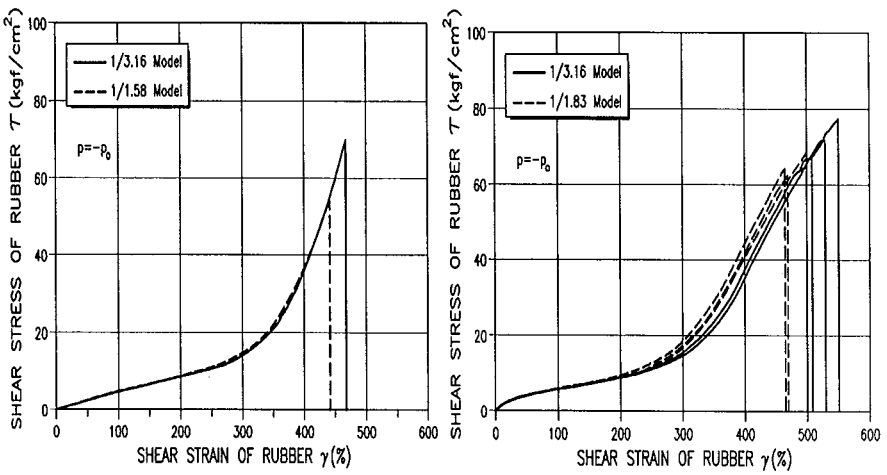

Figure 2. Experimental results for natural and high damping rubber bearing, using reduced scale models (scales 1/3·16, 1/1·58 and 1/1·83)

$\sigma_y = 3{\cdot}06$ kg/cm^2. The dimensions were chosen as being equivalent to the area and total thickness of the rubber component of experimental models with the design specifications shown in Table II.

A plot of horizontal loads versus the horizontal displacements is shown in Figures 3 and 4 for natural rubber bearings and in Figures 5 and 6 for high damping rubber bearings.

Table II. Design specifications of laminated rubber bearing. NRB = Natural Rubber Bearing. HRB = High damping Rubber Bearing (SMiRT11 1991)

Type	NRB	HRB
Diameter (mm)	1600	1420
Area, $\pi \Phi^2/4$ (m^2)	2·0106	1·5837
Height (mm)	440	620
Thickness of rubber sheet (mm)	11·5	8
Number of rubber sheets	19	31
Thickness of steel sheet (mm)	4·5	5·8
Number of steel sheets	18	30
Loading weight, P_0(T)	500	500
Natural horizontal frequency, f_H (Hz)	0·5	0·5
Natural vertical frequency, f_V (Hz)	20	20

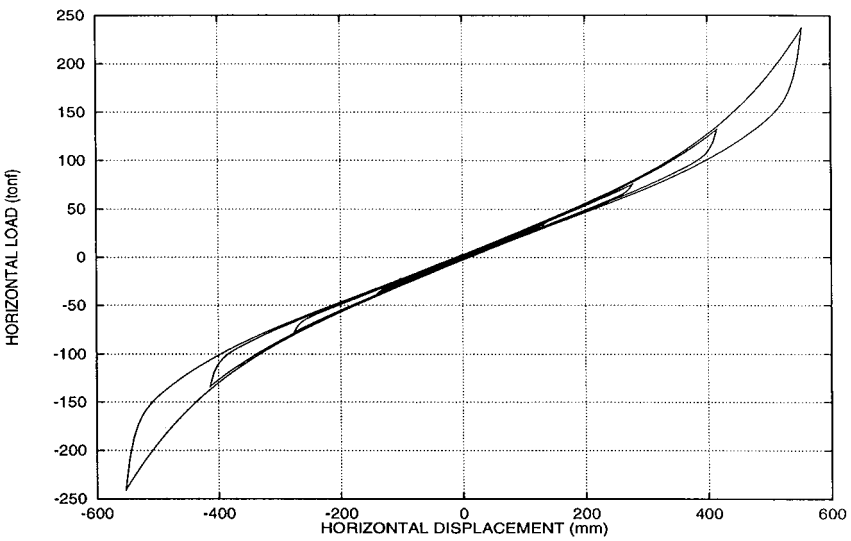

Figure 3. Natural rubber bearing. Numerical model

5. APPLICATION TO A BASE ISOLATED STRUCTURE

As an example, the seismic performance of a six-storey base isolated reinforced concrete frame is compared with a similar fixed-base structure. Maximum inter-storey displacement, absolute floor acceleration and overall indices are used to compare the response of the two structures when both of them are subjected to the N–S component of the El Centro earthquake.

The nodal forces (bending moments, shear and axial forces) in the frame elements are proportional to the inter-storey drift caused by the earthquake, and consequently, these displacements are a measure of possible structural damage. Floor acceleration is an important parameter which

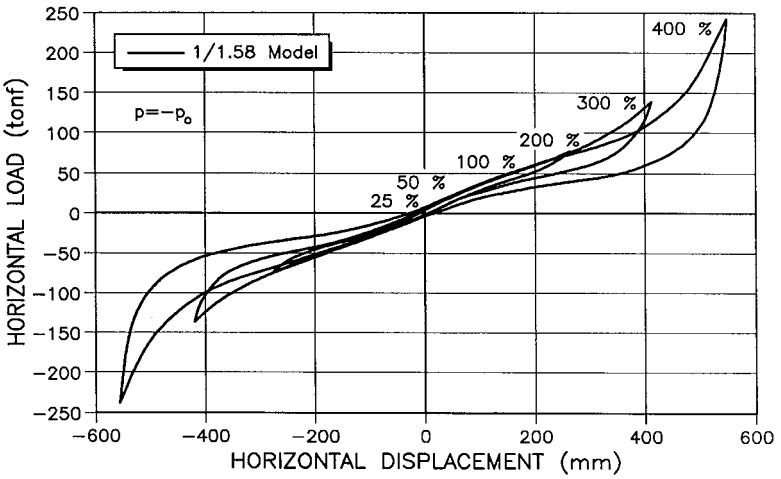

Figure 4. Natural rubber bearing. Experimental results using reduced-scale model (scale 1/1·58)

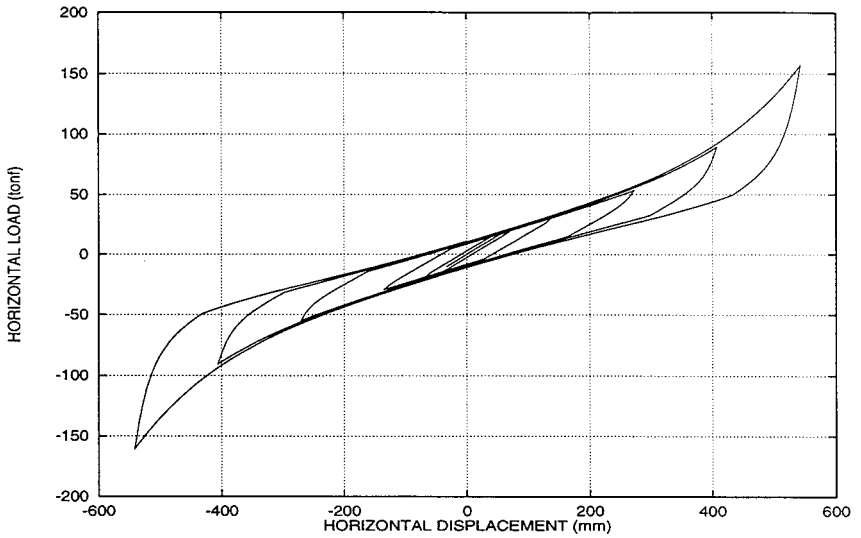

Figure 5. High damping rubber bearing. Numerical model

governs the comfort of people and the damage to the building installations. The overall damage indices enable us to ascertain how far the structures are from elastic behaviour.

5.1. Description of the structural model

Both structures, the base-isolated frame and the fixed-base one, have a first floor 4 m high and five upper floors 3 m high, all of them 10 m wide. The dimensions of the columns and beams are such that the fundamental period is $T = 0{\cdot}54$ s. The stiffness of the columns diminishes with

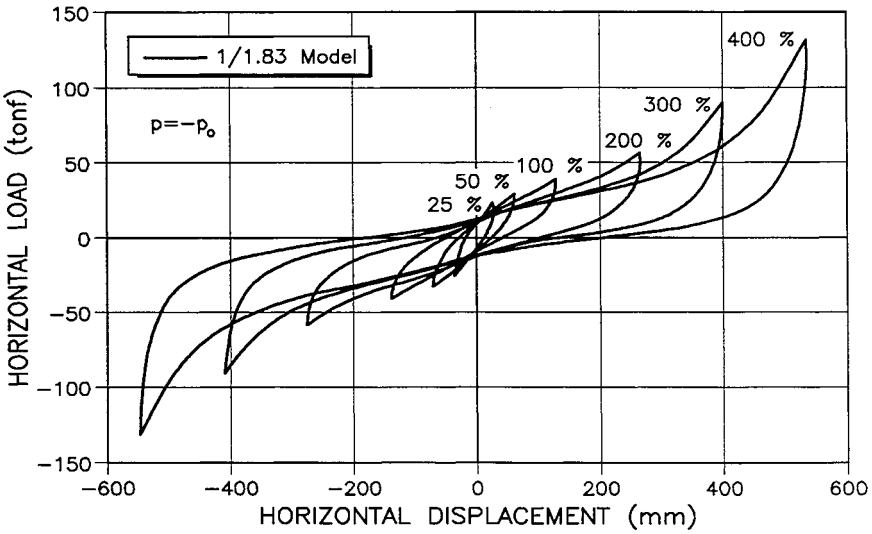

Figure 6. High damping rubber bearing. Experimental results using reduced-scale model (scale 1/1·83)

each storey to achieve this period. The base isolated frame is supported on a HRB with design specifications as shown in Table II.

Because of structural symmetry, only half of the frames are modelled. The columns and beams are modelled using 2D Timoshenko beam elements with their cross-sectional area discretized by layers. Three-nodes quadratic finite elements with three degrees of freedom per node are used. The elements have two Gauss integration points and six layers of the same height and width. In order to model the steel bars, the outer layers ($\frac{1}{3}$ area) are considered as a composed material with two components: concrete (85 per cent) and steel (15 per cent), giving a reinforcement ratio of 4·5 per cent. The inner layers are modelled as a single material, concrete (100 per cent).

Four-node isoparametric plane strain elements are used to model the base and the isolation device. The use of a connection element (see the appendix) allows the base plane elements to work in interaction with the frame bending elements. The material model used here for the rubber pad has the same parameters as the high damping rubber given in the previous section.

The properties of the structural materials, concrete and steel, are included in Table III [30, 31].

The total weight of the structure is 500 T, equally distributed on each of the floor of the structure; the base has a mass equivalent to a single floor.

An important aspect of the seismic base isolation is verified when a displacement is imposed on the isolated and fixed-base structures and the response to free vibration is then compared. The original fixed-base period ($T = 0{\cdot}54$ s) is shifted to a much longer one ($T \approx 1{\cdot}9$ s) close to the design period of the rubber bearing ($T = 2$ s).

5.2. *Seismic analysis*

The earthquake ground motion corresponds to the N–S component of the 1940 El Centro record. The first 12 s of the accelerogram were discretized, with a time increment of 0·02 s.

Table III. Material parameters for concrete and steel

Material	Steel	Concrete
Young modulus, E (kg/cm^2)	$2{\cdot}1 \times 10^6$	$3{\cdot}0 \times 10^5$
Poisson modulus, υ	0·20	0·17
Initial plastic stress, σ^0 (kg/cm^2)	4200	300
Yield criteria	Von Mises	Mohr–Coulomb
Damage model		Kachanov
Initial damage stress, σ^0_{dam} (kg/cm^2)		300
Compression/tension initial ratio, $\sigma^0_{\text{C}}/\sigma^0_{\text{T}}$		10

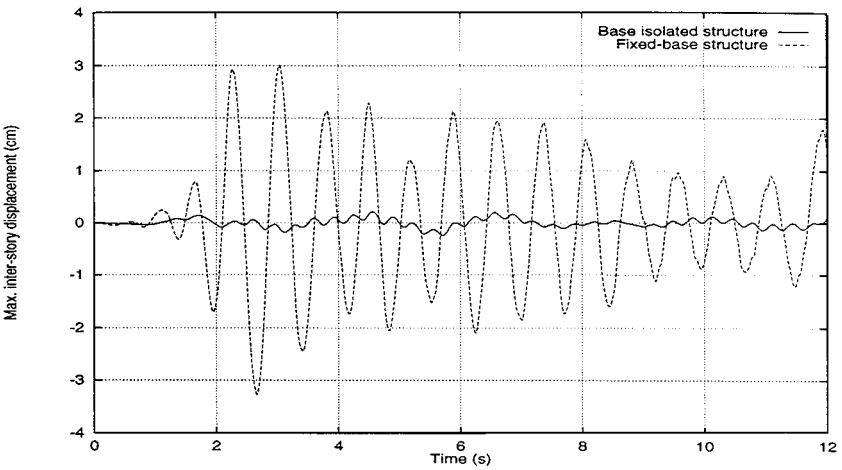

Figure 7. Maximum inter-storey displacement for base isolated and fixed-base structures

Figures 7 and 8 show the maximum inter-storey displacement and the maximum (top floor) absolute structural acceleration for the base isolated and fixed-base structure, respectively. Note that the relative structural displacement for a building equipped with elastomeric rubber bearings is considerably smaller than the corresponding displacement for a conventional fixed-base structure. The same observation can be made regarding acceleration. The maximum values of the response of both structures are shown in Table IV.

Figure 9 illustrates the shear stress of the rubber due to base displacements. The maximum displacement of the base (16·81 cm) correspond to 67·78 per cent shear strain in the rubber pad, far below the breaking point.

In order to evaluate structures subjected to extraordinary actions an overall damage index can be used [30]. The damage index is considered to be local if it refers to a point, or overall if it is applicable to a section, a structural element or to the whole structure. The overall damage index used here considers the local index to be equally weighted at all Gauss points of the structure.

Figure 10 shows these indices for the base isolated and fixed-base structures during the El Centro earthquake. The fixed-base frame shows a very high overall damage index close to 60 per cent. As a result of this damage the building practically fails. In contrast, the base isolated structure suffers

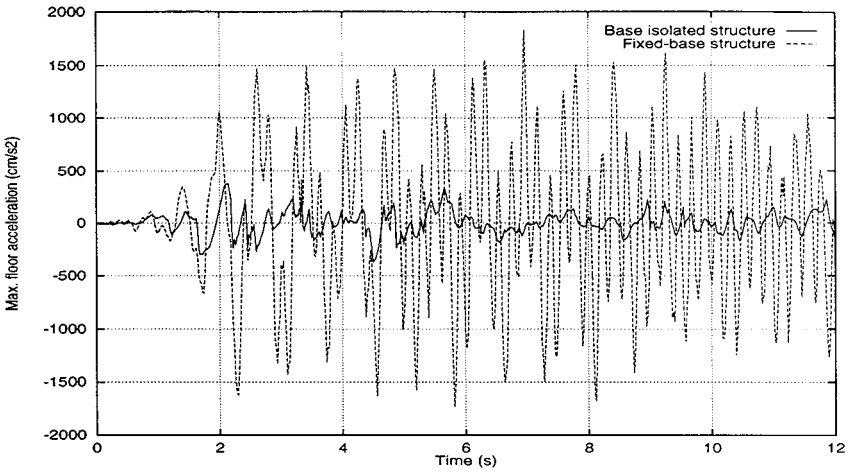

Figure 8. Maximum absolute floor acceleration for base isolated and fixed-base structures

Table IV. Maximum values in the response of base isolated and fixed-base structures to the El Centro earthquake

Structure	Base isolated	Fixed-base
Base displacement (cm)	16·81	0·0
Displacement at top floor (cm)	15·49	16·2
Total structural displacement (cm)	1·53	16·2
Inter-storey displacement (cm)	0·24	3·27
Acceleration at top floor (cm/s^2)	380·8	1831·6

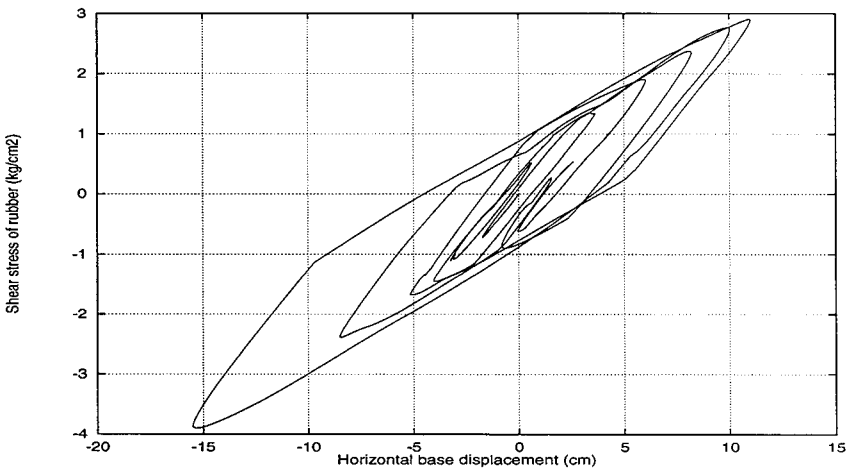

Figure 9. Shear stress of rubber due to base displacement

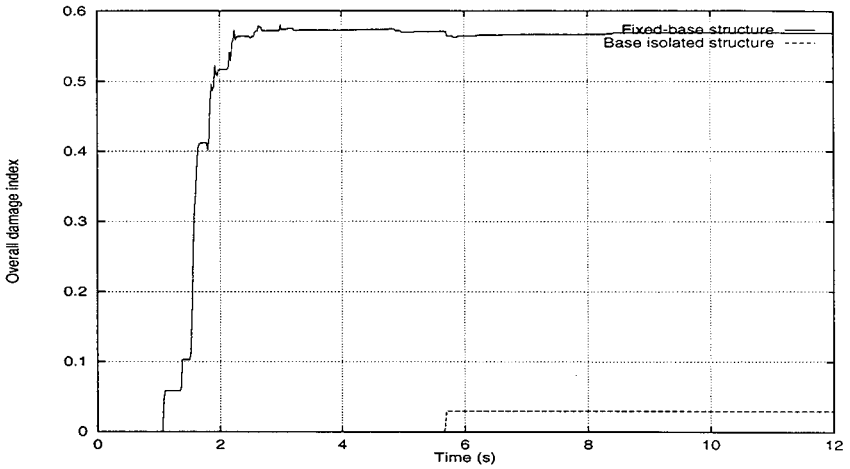

Figure 10. Overall damage indices for base isolated and fixed-base structures

an overall damage index below 3 per cent. Such a low index shows that the structure remains in service after the earthquake, and also that the damage is hardly perceptible by means of visual inspection.

6. CONCLUSIONS

An efficient model to describe the behaviour of rubber-like materials is developed and applied to the analysis of buildings with base isolation devices. Firstly, a hyperelastic phenomenology approach is developed taking into account visco-elasticity as well as plasticity in an additive split of the strain energy function W. Mixing theory is used to incorporate the basic constitutive law for each substance, rubber and carbon black particles, into the overall model. Secondly, an exponential algorithm is applied to update the elastic state of deformation in the elastoplastic formulation. Next, a simple displacement/pressure finite element without additional pressure points is expressed, capable of dealing with the quasi-incompressibility of rubber. Finally, values for the parameters of the model are suggested in order to fit experimental results for laminated elastomeric bearings.

The proposed approach models not only the overall response of elastomeric bearings, but also permits the analysis of complete seismic base isolated buildings. Geometric and material non-linearities are considered, both in the bearing model and in the reinforced concrete structure.

APPENDIX

I.1. Connection element

In order to analyse the whole structure-base isolation system, a connection element has been developed.

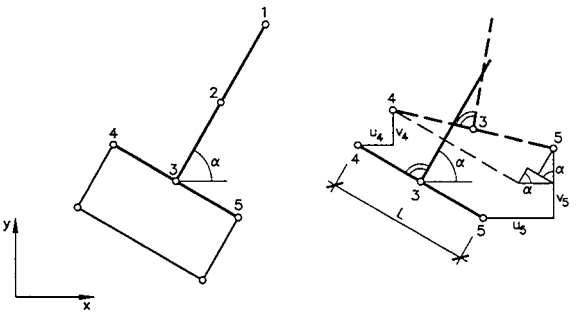

Figure 11. Connection element using a three-nodes beam element and a four-nodes plane one

A beam element is connected to a plane element at the middle point of one of its sides. At the connection point the displacements must be the same. As a consequence, the displacements (u, v) of the node 3 of the beam can be obtained by linear interpolation of the displacements (u, v) of the nodes 4 and 5. The relationship between the rotation at the end of the beam (node 3) and the displacements of nodes 4 and 5 are written accepting that the joint is rigid [32, 33]

$$\begin{bmatrix} u_3 \\ v_3 \\ \theta_3 \end{bmatrix} = \underbrace{\begin{bmatrix} 0{\cdot}5 & 0 & 0{\cdot}5 & 0 \\ 0 & 0{\cdot}5 & 0 & 0{\cdot}5 \\ -\cos\alpha/L & -\sin\alpha/L & \cos\alpha/L & \sin\alpha/L \end{bmatrix}}_{m} \cdot \begin{bmatrix} u_4 \\ v_4 \\ u_5 \\ v_5 \end{bmatrix} \tag{61}$$

Using this equation, the relationship between the displacement fields of the beam and of the connection element is

$$\mathbf{u}_{\text{beam}} = \begin{bmatrix} u_1 \\ v_1 \\ \theta_1 \\ u_2 \\ v_2 \\ \theta_2 \\ u_3 \\ v_3 \\ \theta_3 \end{bmatrix}_{(9\times 1)} = \underbrace{\begin{bmatrix} \mathbf{I}_{(6\times 6)} & \mathbf{0} \\ \mathbf{0} & \mathbf{m}_{(3\times 4)} \end{bmatrix}}_{\mathbf{T}_{(9\times 10)}} \cdot \begin{bmatrix} u_1 \\ v_1 \\ \theta_1 \\ u_2 \\ v_2 \\ \theta_2 \\ u_4 \\ v_4 \\ u_5 \\ v_5 \end{bmatrix}_{(10\times 1)} = \mathbf{T} \cdot \mathbf{u}_{\text{con}} \tag{62}$$

The forces at the end of the beam can be related to the forces at nodes 4 and 5 of the plane element in a similar way

$$\underbrace{\begin{bmatrix} 0{\cdot}5 & 0 & -\cos\alpha/L \\ 0 & 0{\cdot}5 & -\sin\alpha/L \\ 0{\cdot}5 & 0 & \cos\alpha/L \\ 0 & 0{\cdot}5 & \sin\alpha/L \end{bmatrix}}_{\mathbf{m}^{\mathrm{T}}} \cdot \begin{bmatrix} H_3 \\ V_3 \\ M_3 \end{bmatrix} = \begin{bmatrix} H_4 \\ V_4 \\ H_5 \\ V_5 \end{bmatrix} \tag{63}$$

Denoting $\mathbf{F}_{\text{beam}}$ the force vector of the standard beam element and $\mathbf{F}_{\text{con}}$ the same for the connection element, the relationship between both is $\mathbf{T}^{\text{T}}\mathbf{F}_{\text{beam}} = \mathbf{F}_{\text{con}}$. Forces and displacements are related through the stiffness matrix

$$\mathbf{K}_{\text{beam}_{(9\times 9)}} \cdot \mathbf{u}_{\text{beam}} = \mathbf{F}_{\text{beam}} \rightarrow \underbrace{\mathbf{T}^{T} \cdot \mathbf{K}_{\text{beam}} \cdot \mathbf{T}}_{\mathbf{K}_{\text{con}_{(10\times 10)}}} \cdot \mathbf{u}_{\text{con}} = \mathbf{F}_{\text{con}} \tag{64}$$

where $\mathbf{K}_{\text{con}}$ is the stiffness matrix of the connection element.

ACKNOWLEDGEMENTS

Support for this work was provided by a grant from Universidad Nacional del Nordeste, Argentina. This support is gratefully acknowledged.

REFERENCES

1. SMiRT11. *Seismic Isolation and Response Control for Nuclear and Non-Nuclear Structures*. Structural Mechanics in Reactor Technology, SMiRT11, Tokyo, 1991.
2. Skinner RI, Robinson WH, McVerry G. *An Introduction to Seismic Isolation*. Wiley: Chichester, 1993.
3. Barbat AH, Bozzo LM. Seismic analysis of base isolated buildings. *Archives of Computational Methods in Engineering* 1997; **4**(2):153–192.
4. Kelly JM. *Dynamic and Failure Characteristics of Bridgestone Isolation Bearings*. Earthquake Engineering Research Center, College of Engineering, University of California at Berkeley, 1991.
5. Kelly JM. *Final Report on the International Workshop on the Use of Rubber-Based Bearing for the Earthquake Protection of Buildings*. Earthquake Engineering Research Center, College of Engineering, University of California at Berkeley, 1995.
6. Koh CG, Kelly JM. Viscoelastic stability model for elastomeric isolation bearings. *Journal of Structural Engineering* 1989; **115**(2):285–302.
7. Ali HM, Abdel-Ghaffar AM. Modelling of rubber and lead passive-control bearings for seismic analysis. *Journal of Structural Engineering* 1995; **121**(7):1134–1144.
8. Fuller KNG, Gough J, Pound TJ, Ahmadi HR. High damping natural rubber seismic isolators. *Journal of Structural Control* 1997; **4**(2):19–40.
9. Hwang JS, Ku SW. Analytical modelling of high damping rubber bearings. *Journal of Structural Engineering* 1997; **123**(8):1029–1036.
10. Molinares N, Barbat AH. *Edificios con aislamiento de base no lineal*. Monografías de Ingeniería Sísmica 5, Centro Internacional de Métodos Numéricos en Ingeniería, CIMNE, Barcelona, 1994.
11. Barbat AH, Miquel-Canet J. *Estructuras Sometidas a Acciones Sísmicas*. Centro Internacional de Métodos Numéricos en Ingeniería, CIMNE, Barcelona, 1994.
12. Nagarajaiah S, Reinhorn AM, Constantinou MC. Nonlinear dynamic analysis of 3-D-Base-isolated structures. *Journal of Structural Engineering* 1991; **117**(7):2035–2054.
13. Nagarajaiah S, Li C, Reinhorn A. Constantsnou M. 3D-BASIS-TABS: version 2.0 computer program for nonlinear dynamic analysis of three dimensional base isolated structures. *Technical Report NCEER-94-0018*, National Center for Earthquake Engineering Research, University at Buffalo, 1994.
14. Herrmann LR, Hamidi R, Shafigh-Nobari F, Lim CK. Nonlinear behavior of elastomeric bearings. I: Theory. *Journal of Engineering Mechanics* 1988; **114**(11):1811–1830.
15. Moore JK. A nonlinear finite element analysis of elastomeric bearings. *Ph.D. thesis*, Department of Civil Engineering, University of California at Davis, 1982.
16. Herrmann LR, Hamidi R, Shafigh-Nobari F, Ramaswamy A. Nonlinear behavior of elastomeric bearings. II: FE analysis and verification. *Journal of Engineering Mechanics* 1998; **114**(11):1831–1853.
17. Oller S, Oñate E, Miquel J, Botello S. A plastic damage constitutive model for composite materials. *International Journal of Solids and Structures* 1996; **33**(17):2501–2518.
18. Barbat A, Oller S, Oñate E, Hanganu A. Viscous damage model for Timoshenko beam structures. *International Journal of Solids and Structures* 1997; **34**(30):3953–3976.
19. Ogden RW. *Non-Linear Elastic Deformations*. Ellis Horwood: Chichester, England, 1984.
20. Morman K. The generalized strain measure with application to non-homogeneous deformations in rubber-like solids. *Journal of Applied Mechanics* 1986; **53**:726–728.

21. Simo JC, Taylor RL. Quasi-incompressible finite elasticity in principal stretches. Continuum basis and numerical algorithms. *Computer Methods in Applied Mechanics and Engineering* 1991; **85**:273–310.
22. Govindjee S, Simo JC. Mullins' effect and the strain amplitude dependence of the storage modulus. *International Journal of Solids and Structures* 1992; **29**(14/15):1737–1751.
23. Kaliske M, Gebbeken N, Rothert H. A generalized approach to inelastic behaviour at finite strains-Application to polymeric material. *Proceedings of the Fifth International Conference on Computational Plasticity*, Centro Internacional de Métodos Numéricos en Ingeniería, CIMNE: Barcelona, 1997:937–944.
24. Salomón O, Oller S, Barbat A. Modelling of laminated elastomeric passive-control bearing for seismic analysis. *Fourth World Congress on Computational Mechanics*, Buenos Aires, Argentina, 1998.
25. Simo JC. Algorithms for static and dynamic multiplicative plasticity that preserve the classical return mapping schemes of the infinitesimal theory. *Computer Methods in Applied Mechanics and Engineering* 1992; **99**:61–112.
26. Sussman T, Bathe K. A finite element formulation for nonlinear incompressible elastic and inelastic analysis. *Computers and Structures* 1987; **26**(1/2):357–409.
27. Gadala MS. Alternative methods for the solution of hyperelastic problems with incompressibility. *Computers and Structures* 1992; **42**(1)1–10.
28. Bathe KJ. *Finite Element Procedures*. Prentice-Hall: NJ, 1996.
29. Simo JC. A framework for finite strain elastoplasticity based on maximum plastic dissipation and the multiplicative decomposition: Part 2 Computational aspects. *Computer Methods in Applied Mechanics and Engineering* 1988; **68**:1–31.
30. Hanganu DA. Análisis no lineal estático y dinámico de estructuras de hormigón armado mediante modelos de daño. *Ph.D. Thesis*, Escuela Tecnica Superior de Ingenieros de Caminos Canales y Puertos de Barcelona, Universidad Politécnica de Cataluña, 1997.
31. Oller S. *Modelización Numérica de Materiales Friccionales*. Monografía 3, Centro Internacional de Métodos Numéricos en Ingeniería, CIMNE, Barcelona, 1991.
32. Oñate E. *Cálculo de Estructuras por el Método de los Elementos Finitos*. Centro Internacional de Métodos Numéricos en Ingeniería, CIMNE, Barcelona, 1992.
33. Salomón O. Estructuras con sistema de aislamiento sísmico. Análisis por elementos finitos. *Master's Thesis*, Escuela Técnica Superior de Ingenieros de Caminos Canales y Puertos de Barcelona, Universidad Politécnica de Cataluña, 1995.

